communications earth & environment

ARTICLE

https://doi.org/10.1038/s43247-023-00983-3 OPEN

A thicker Antarctic ice stream during the mid-Pliocene warm period

Martim Mas e Braga[1,2,15✉], Richard S. Jones[3], Jorge Bernales[4], Jane Lund Andersen[1,5], Ola Fredin[6], Mathieu Morlighem[7], Alexandria J. Koester[8], Nathaniel A. Lifton[8,9], Jonathan M. Harbor[1,2,8,10], Yusuke Suganuma[11], Neil F. Glasser[12], Irina Rogozhina[13,14] & Arjen P. Stroeven[1,2]

Ice streams regulate most ice mass loss in Antarctica. Determining ice stream response to warmer conditions during the Pliocene could provide insights into their future behaviour, but this is hindered by a poor representation of subglacial topography in ice-sheet models. We address this limitation using a high-resolution model for Dronning Maud Land (East Antarctica). We show that contrary to dynamic thinning of the region's ice streams following ice-shelf collapse, the largest ice stream, Jutulstraumen, thickens by 700 m despite lying on a retrograde bed slope. We attribute this counterintuitive thickening to a shallower Pliocene subglacial topography and inherent high lateral stresses at its flux gate. These conditions constrict ice drainage and, combined with increased snowfall, allow ice accumulation upstream. Similar stress balances and increased precipitation projections occur across 27% of present-day East Antarctica, and understanding how lateral stresses regulate ice-stream discharge is necessary for accurately assessing Antarctica's future sea-level rise contribution.

[1] Department of Physical Geography, Stockholm University, Stockholm, Sweden. [2] Bolin Centre for Climate Research, Stockholm University, Stockholm, Sweden. [3] Securing Antarctica's Environmental Future, School of Earth, Atmosphere and Environment, Monash University, Melbourne, Australia. [4] Institute for Marine and Atmospheric Research, Utrecht University, Utrecht, Netherlands. [5] Department of Geoscience, Aarhus University, Aarhus, Denmark. [6] Department of Geoscience and Petroleum, Norwegian University of Science and Technology, Trondheim, Norway. [7] Department of Earth Sciences, Dartmouth College, Hanover, NH, USA. [8] Department of Earth, Atmospheric, and Planetary Sciences, Purdue University, West Lafayette, IN, USA. [9] Department of Physics and Astronomy, Purdue University, West Lafayette, IN, USA. [10] Purdue University Global, West Lafayette, IN, USA. [11] National Institute of Polar Research, Tokyo, Japan. [12] Centre for Glaciology, Department of Geography and Earth Sciences, Aberystwyth University, Aberystwyth, UK. [13] Department of Geography, Norwegian University of Science and Technology, Trondheim, Norway. [14] Center for Advanced Research in Arid Zones (CEAZA), La Serena, Chile. [15] Present address: School of Geography and Sustainable Development, The University of St Andrews, St Andrews, UK. ✉email: mmeb1@st-andrews.ac.uk

The mid-Pliocene warm period (3.3–3.0 Ma, hereafter referred to as the Pliocene) marks the last time in Earth's history that atmospheric CO_2 levels were as high as today[1]. For this reason, it is often treated as an analogue for how the polar ice sheets might respond to future warming. In sectors where the Antarctic Ice Sheet (AIS) is grounded below sea level, evidence shows that substantial ice loss occurred during periods when global temperatures rose above modern values[2–5]. Loss of grounded ice leads to an input of freshwater to the oceans and an increase in global mean sea level. During the Pliocene, ice loss from both the AIS and Greenland Ice Sheet is thought to have led to a global mean sea level over 20 m higher than today[6,7]. It is, however, unclear whether a future climate similar to the Pliocene would result in a sea-level rise of the same magnitude.

The main mechanism for AIS mass loss is the dynamic thinning of ice streams[8]. Dynamic thinning refers to the thinning of grounded ice due to increased ice flux towards the ice sheet margin. In Antarctica, most ice streams become floating ice shelves at the coast. When an ice shelf is laterally confined or anchored at its base by submarine topographic highs (known as pinning points), the dominant longitudinal stresses result in force being applied against the ice stream, creating a buttressing effect. Buttressing is directly affected by the ice shelf geometry[9] and decreases through thinning and calving[10,11]. This decrease in buttressing induces an increased ice flux through the grounding line[12] and upstream ice acceleration, leading to dynamic thinning[13]. Areas where ice is grounded below sea level and where the subglacial topography deepens toward the ice sheet interior (known as a retrograde bed slope) are particularly sensitive to ice mass loss because such conditions can trigger a process called marine ice sheet instability[14], provided other conditions are met[15–18]. This instability is triggered because of the increased ice sheet thickness at the grounding line (the point where grounded ice becomes afloat) as it retreats inland along the retrograde slope, resulting in increased ice flux. The increased ice flux may cause a positive feedback of ever-increasing mass loss until the grounding line reaches a slope that shallows towards the interior. However, models and observations show that this process does not apply in all cases due to geometrical variations and stabilising mechanisms on the stress balance[16–19]. Today, rapid retreat is most evident in the West Antarctic Ice Sheet (WAIS)[20,21]. This is partly because the WAIS is more exposed to ocean-driven melt by warmer water masses than the East Antarctic Ice Sheet (EAIS)[22] and because the bedrock topography beneath the WAIS lies largely below sea level, with a deeper bed under its interior than under its margins[23]. Conversely, responses along the EAIS margin vary significantly from basin to basin[8] due to variations in ocean circulation and in the extent to which basins are grounded below sea level, including variations in their bed slope[24].

During the Pliocene, the EAIS interior is generally thought to have been thicker than at present[4,25]. A warmer atmosphere carries more moisture[11], which leads to increased snowfall over the ice sheet[26] and could have resulted in increased accumulation over the EAIS interior. This interpretation is in line with surface-exposure ages, which indicate that during the Pliocene Dronning Maud Land (DML), Mac Robertson Land, and the central Transantarctic Mountains had thicker (>600 m) ice cover in mountain ranges that are partially ice-free today (called nunataks)[27,28]. At the EAIS margins, available numerical models and empirical evidence indicate that the EAIS response to Pliocene warmth was less uniform. Areas where the ice sheet was largely grounded below sea level at the time are thought to have collapsed or retreated significantly, producing a steeper elevation profile[5,25,29,30]. The response of marginal sectors that lie mostly above sea level, however, is less constrained due to a lack of empirical evidence[24].

The potential for mass gains in regions of the AIS during warm periods needs to be well understood and constrained. This is because, in current projections, increased accumulation under a warmer climate partially offsets the loss of grounded ice from the WAIS and elsewhere[31], and the balance between current surface mass balance gains and dynamic losses is highly uncertain[24]. Western DML offers an ideal setting for evaluating the EAIS response to past warm periods. It contains areas where ice is grounded both above and below sea level, and modern estimates of mass balance show this region to be gaining mass over its interior (Fig. 1)[32], in line with Pliocene reconstructions of nearby areas[27,33]. Specifically, ice core, surface exposure, and geophysical data offer constraints on the EAIS configuration in this region, supporting a thicker interior and thinner margins during interglacials[34,35].

The steep and variable topography of DML, however, is not captured by continent-scale ice sheet models. Furthermore, recently discovered areas where the subglacial topography is over-deepened are also not included in most recent models[24,36]. These models are usually run at low spatial resolutions to achieve long simulation times and consequently cannot represent regional patterns of ice dynamics, especially over areas of steep subglacial topography[37,38]. This inability can at least partially explain why such models do not capture the timing and magnitude of ice thinning recorded by geological constraints[39,40]. At the same time, such constraints, which are discrete in space, are extrapolated over a large area using assumptions based on the modern ice sheet geometry and potentially miss important regional variations.

To assess how western DML ice streams respond to a warmer climate such as the Pliocene, we use a high-resolution numerical model[41] to simulate the region's ice streams, with a particular focus on Jutulstraumen, its largest ice stream (Fig. 1). We simulate the response of the entire Jutulstraumen catchment to the Pliocene climate using five of the coupled atmosphere–ocean global climate models from the Pliocene Model Intercomparison Project Phase 1: HadCM3[25,42], COSMOS[43], IPSLCM5A[44], MIROC4m[45], and MRI-CGCM2.3[46]. These models have been used in other studies of the Pliocene AIS[25,47], and here we make use of an updated mid-Pliocene subglacial topography reconstruction[48]. We model equilibrium-state Pliocene ice sheet geometries and show that most ice streams in DML were thinner than today, while Jutulstraumen was thicker under a warmer climate than at present. We also evaluate to which degree the modern over-deepened subglacial topography[23,36] presents a risk for ice stream vulnerability[49] because its response depends on the degree of ocean warming and ice-shelf buttressing. Finally, we identify that ten East Antarctic ice streams (including Jutulstraumen) have similar topographical settings and are located where snowfall is projected to increase until 2100. Thus, these ice streams should be more closely monitored regarding their responses to future climate change.

Results

Contrasting responses between ice streams during the Pliocene. All five model reconstructions of the Pliocene show dynamic thinning at Schyttbreen (the ice stream west of Jutulstraumen) in the absence of ice shelf buttressing (Fig. 2). The grounding line is located 10–20 km further inland than at present, the ice surface is up to 300 m lower at its flux gate (here defined as the section of the ice stream's grounding line through which most ice flows), and dynamic thinning reaches as far as 100 km inland. Dynamic thinning is also inferred as the norm for other ice streams in western DML, as shown by a lower-resolution experiment (see Methods) that includes all ice streams west of Schyttbreen to

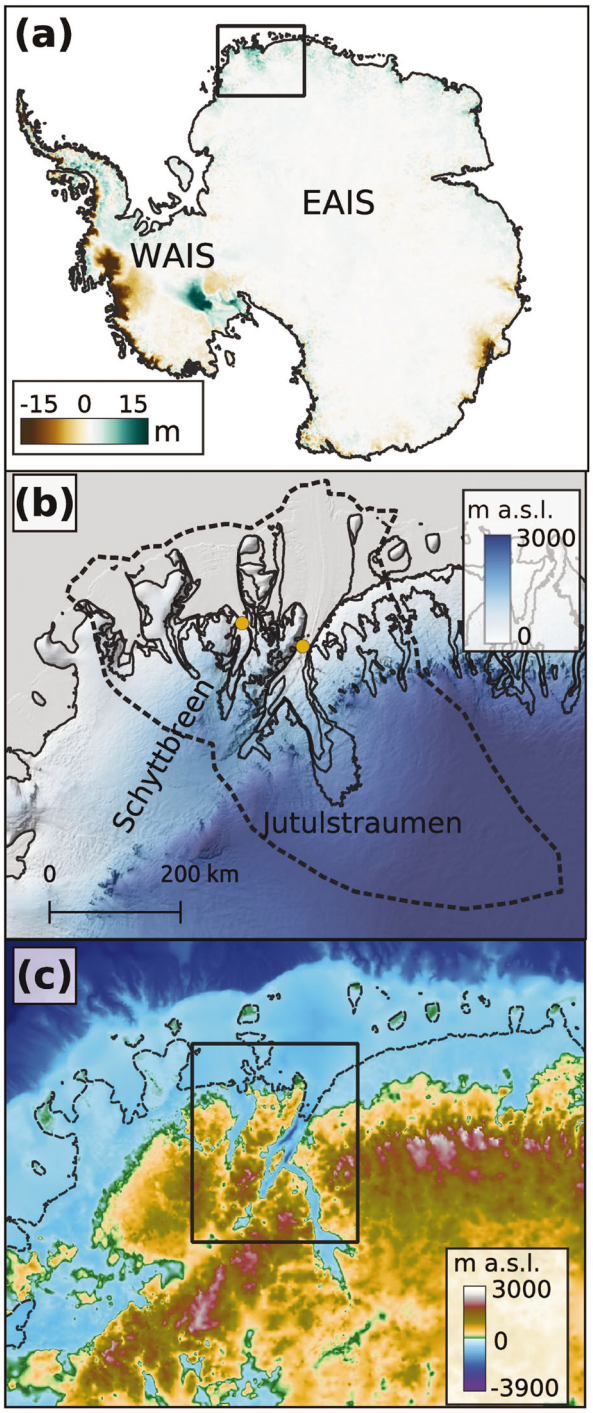

Fig. 1 Overview of DML and Jutulstraumen. a Grounded ice elevation changes between January 1994 and December 2020 from ITS_LIVE[84], black rectangle highlights the DML area displayed in panels (**b**, **c**); WAIS and EAIS stand for West and East Antarctic Ice Sheet, respectively. **b** Contemporary ice-surface elevation (colours)[23] and ice surface speed contours[65] (solid lines denoting 20, 50, and 100 ma^{-1} increasing towards the margins). Shading highlights the steep topographic gradient between the ice sheet interior and the margin. Yellow dots mark the flux gates where elevation changes in Fig. 7 were computed. A thick dashed line marks the modelled domain, and a thin solid line shows the modern grounding line. **c** Modern subglacial topography[23], including an updated dataset for Jutulstraumen[36]; black rectangle highlights the area shown in Figs. 2 and 6 (smaller-domain experiments) while Fig. 3 (larger-domain experiment) covers the full extent of panel **c**. The thin dashed line marks the modern grounding line.

Veststraumen (Figs. 3 and 4). Like Schyttbreen, these ice streams rest on retrograde bed slopes and are grounded below sea level at their margins.

Jutulstraumen, however, shows the opposite response. Despite being separated from Schyttbreen by only 40 km, it is up to 700 m thicker under all modelled Pliocene scenarios (Fig. 2). Ice surface elevations higher than present are visible along its entire extent even in the absence of buttressing from its ice shelf, which either collapses (Fig. 2a, d) or is significantly thinner (Fig. 2b, c, e) depending on the forcing. Jutulstraumen thickens most just upstream of its present-day flux gate and along its western tributary, Penck Trough. Consequently, the Pliocene grounding line is located further downstream, at a point where it no longer forms an embayment inland but rather produces a smooth grounded-ice margin. Ice thickening varies from ~700 m over Jutulstraumen's flux gate and ~600 m across the bounding nunatak ranges (i.e., the nunataks along the ice stream, such as those that separate Jutulstraumen and Schyttbreen) to ~ 350 m inland. A thicker ice stream in DML is restricted to Jutulstraumen and is also observed in the larger-domain experiment (Fig. 3). In both smaller and larger domains, the ice surface is higher than at present around the nunataks, outside of the streaming regions, with a thickening of 400–600 m (Figs. 2 and 3) that is consistent with geological reconstructions in the mountain ranges of central DML[27,35].

Mechanisms for a thicker ice stream. The Pliocene subglacial topography of the contrasting thinner and thicker ice streams, Schyttbreen and Jutulstraumen, differ in key aspects (Fig. 3b). Schyttbreen has a relatively flat and wide bed close to its grounding line, whereas Jutulstraumen exhibits a narrower and deeper flux gate. This pattern is evident both in their reconstructed Pliocene[48] and modern subglacial topographies[23] (compare Figs. 1c and 3b). Both ice streams are forced with the same Pliocene surface mass balance (Fig. 5) and their ice shelves undergo the same degree of basal melt (see Methods), which implies that their subglacial topography is the main contrasting condition. The lateral strain rates along the flux-gate margins of Jutulstraumen are higher than at Schyttbreen and peak over a longer distance (Fig. 6), creating a topographic bottleneck effect. The high strain rates along the western margin of Jutulstraumen are evident by the rifts and crevasses observed in contemporary satellite imagery[50], reflecting the strong lateral stresses exerted by the bounding mountain topography. Further end-member tests where lateral stresses were greatly reduced within plausible assumptions, either due to a much warmer ice[51] or even further weakened ice-stream margins due to shear heating[52], did not prevent the thickening of Jutulstraumen (Supplementary Note 1). We thus infer that inherent high lateral stresses provide enough resistance against ice flow to reduce discharge through the flux gate and prevent runaway retreat of the grounding line under reduced ice shelf buttressing and a retrograde bed slope. This flow constriction, in turn, reduces dynamic thinning[19,53], or, as in our Pliocene experiments, allows for a thicker ice stream. Consequently, Jutulstraumen's bottleneck reduces how much grounded ice can be lost compared with the other ice streams, and therefore the ice stream responds to a warmer climate in a way similar to the less dynamic mountain regions that flank it.

While Jutulstraumen's grounding line does not retreat after the loss of ice-shelf buttressing due to high lateral drag, the thickening of the ice stream under late Pliocene climate conditions is also a result of its shallower topography and increased accumulation upstream of its flux gate. Such changes are not necessarily restricted to the Pliocene and possibly occurred throughout the Quaternary. While the AIS as a whole

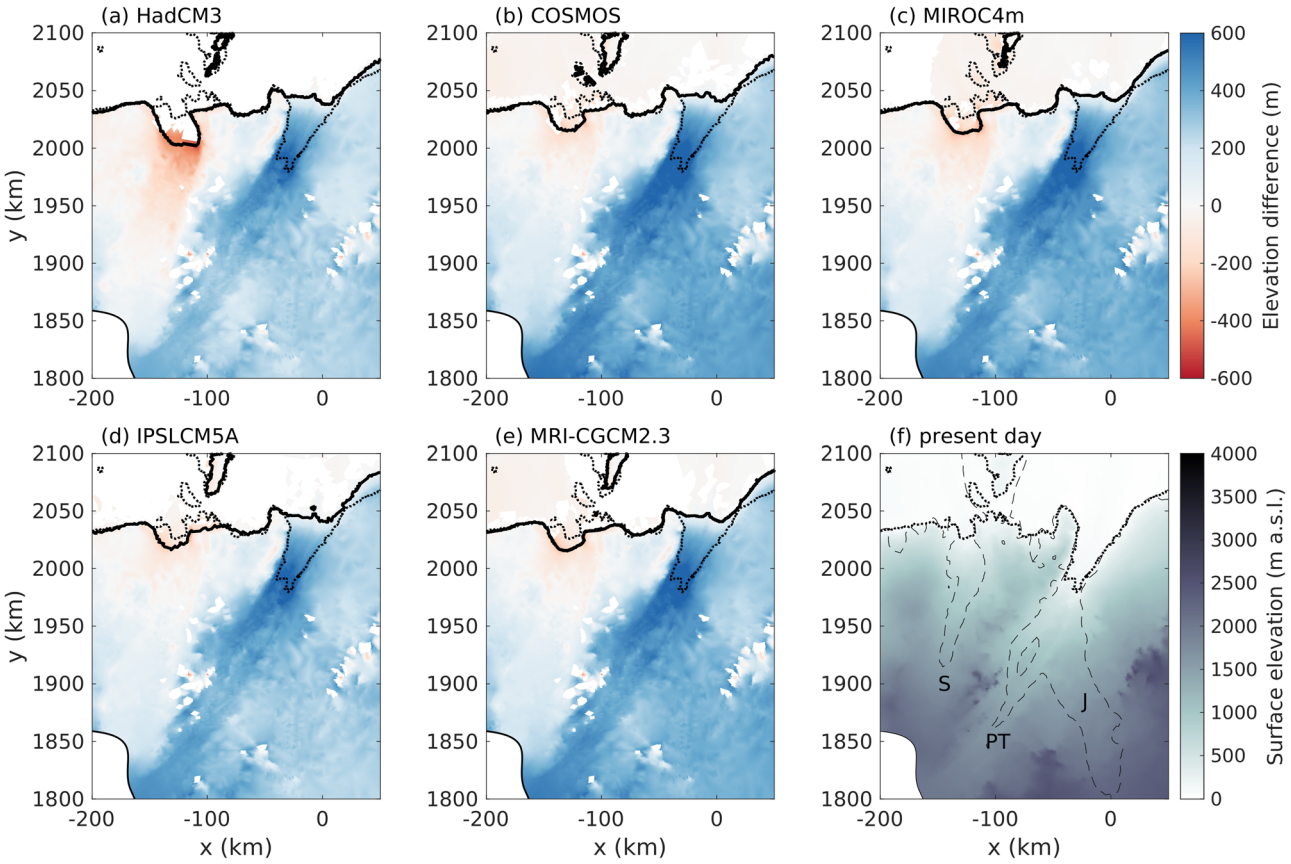

Fig. 2 Jutulstraumen is thicker under all climate forcings. a–e Ice–surface elevation differences between all Pliocene-forced experiments and present day[23] (panel **f**). Panel (**f**) also shows the 50 ma^{-1} surface speed contour as dashed grey lines, highlighting the ice streams, which are marked with S (Schyttbreen), PT (Penck Trough), and J (Jutulstraumen). Black dashed lines in all panels show the modern grounding-line position, while black solid lines show the modelled Pliocene position.

was demonstrated to become increasingly unstable throughout geological time due to the evolution of its subglacial topography[49], geological reconstructions support the notion that the ice sheet surface over the mountains in DML has progressively lowered since the Pliocene[27,35] as a result of surface cooling in the Subantarctic South Atlantic (the moisture-source region for DML[54,55]). A cooler ocean does not provide as much moisture to the atmosphere, and snowfall therefore decreases over the ice sheet interior. In the Holocene, records of both Subantarctic South Atlantic sea-surface temperatures[55] and accumulation rates over the DML ice sheet interior[56] indicate a shift from a decreasing to an increasing trend in accumulation at some point between 5 and 3.8 ka. The current observed thickening over Jutulstraumen (Fig. 1a)[32] could therefore be a response to increased Holocene accumulation.

Future drivers of ice-stream thickness changes. Recent studies show that EAIS mass gains caused by increased snow accumulation outweigh losses driven by ocean warming over most drainage basins[31,32,57]. This is particularly true for Jutulstraumen, where mass-balance estimates from gravimetry show an acceleration of mass gain[32], in line with increased accumulation over the DML plateau due to atmospheric warming[26,57]. Our Pliocene findings predict that Jutulstraumen would thicken further with future atmospheric warming and increased accumulation. However, one key difference exists between the Pliocene and the contemporary ice sheet, which needs further consideration: the subglacial topography has evolved substantially, primarily because of continuous subglacial erosion by the active ice streams. Crucially, at its flux gate, the modern Jutulstraumen basal topography[23] is up to 1000 m deeper than in the Pliocene[48] but has approximately the same width (compare Figs. 1c and 3b). This calls into question whether the lateral stresses at its narrow flux gate can also prevent runaway grounding-line retreat over the modern subglacial topography and whether the conclusions drawn from our Pliocene experiments hold for the modern AIS. To test the implications of this difference for contemporary ice streams in terms of its grounding-line migration, we perform an ensemble of 21 experiments using two different parameterisations for ice-shelf basal melting (see Methods, section "Response of the modern ice sheet to future-like ocean scenarios"; Supplementary Table 1). These experiments include seven different basal-melting scenarios representative of modern and Pliocene conditions, combined with three upper-end sea-level rise scenarios. They are run for 1000 years starting from the present-day configuration and surface mass balance, under constant ice-shelf basal melting, and sea level rising over the first 300 years. Remarkably, Jutulstraumen thickens dynamically, and its grounding line does not retreat despite sea-level rise in all cases where its ice shelf remains significantly extensive, either confined by the narrow flux-gate topography and/or dynamically anchored by pinning points further downstream (blue markers in Fig. 7b, which refer to the experiments in Fig. 8a–c). However, the same is not observed in the cases where ocean warming, affecting both basal melting and calving, is high enough to completely collapse its ice shelf or reduce it to the point where it is no longer laterally confined or anchored by pinning points. In contrast to the Pliocene simulations, Jutulstraumen becomes thinner in all cases where ice shelf buttressing is reduced.

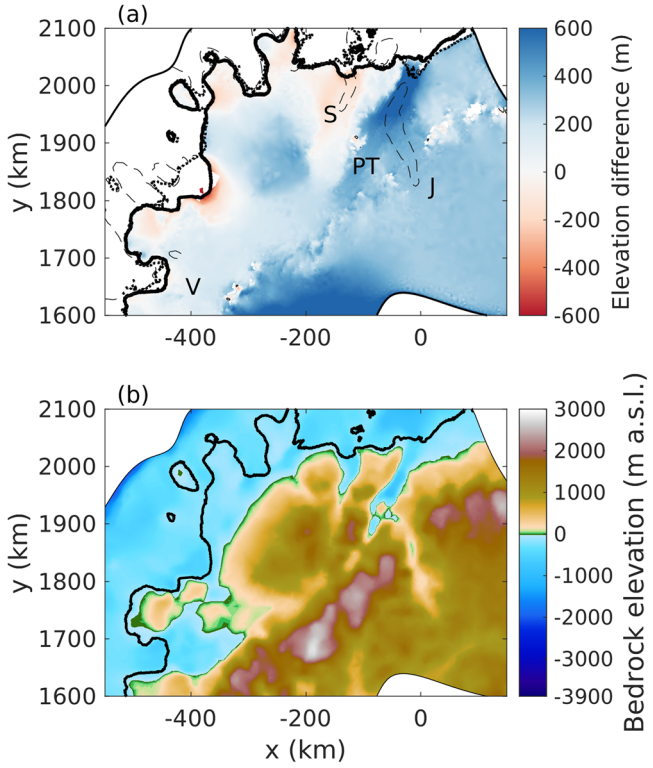

Fig. 3 Dynamic thinning is the norm for western DML ice streams. **a** Ice-surface elevation difference between the Pliocene (forced by HadCM3) and today, for the larger model domain that includes ice streams west of Jutulstraumen. The dashed line indicates the 50 ma^{-1} surface speed contour, and the ice streams discussed in the text are indicated by their initials (Fig. 2f; V for Veststraumen). **b** Pliocene subglacial topography[48]. Dotted lines in panel **a** show the relaxed present-day grounding line, while solid lines in panels **a** and **b** show their modelled Pliocene position.

The interplay between ice-shelf buttressing and changes in ice thickness and extent is not straightforward[58]. Nevertheless, the normal buttressing ratio (Θ_N)[59] is a useful way to illustrate the role of ice-shelf buttressing in these experiments and shows that Jutulstraumen and Schyttbreen have completely different responses to the demise of their ice shelves (Fig. 7). In short, Θ_N quantifies how large normal stresses are at the grounding line compared to a hypothetical case where ice shelves are absent. Values above 1, albeit non-physical, indicate a stress balance that promotes increased flux through the grounding line into the ice shelf at the specific region over which it was calculated[59], while values below 1 indicate that stresses are acting to buttress ice flow across the grounding line. The present-day configuration of the trough in which Jutulstraumen sits, which laterally confines both grounded and floating ice, prevents dynamic thinning only until its ice shelf becomes unanchored (Fig. 8). When the ice shelf no longer buttresses Jutulstraumen, the effect of its deeper trough outweighs the counteracting effect of lateral drag at the flux gate, and mass loss occurs. Schyttbreen, as expected, is more sensitive: it does not need a significant reduction of its ice shelf and consequent loss of buttressing to trigger dynamic thinning.

Discussion

The findings from our modelling experiments have implications for interpreting geological reconstructions of past ice sheet change and for evaluating the future response of EAIS ice streams. Compared with the ice streams that thinned under warmer conditions, the modelled ice thickness response was different at the Nunatak ranges, where several mountain summits are exposed (white areas where ice is grounded in Fig. 2). Geological records of past ice stream change are commonly collected from nunatak ranges, yet we show that the ice surface evolves differently in these less dynamic regions than over most ice streams. Whereas higher modelled ice-surface elevations around nunataks are consistent with empirical reconstructions[27,35], our results also highlight that dynamic thinning of ice streams such as at Schyttbreen and its western neighbours can be easily overlooked in the geological record. This distinction is true for Antarctica but equally true for exposure-age constraints in other mountainous regions that have been covered by ice sheets in the past. Therefore, when interpreting geological records, one should not treat all nunataks similarly. Instead, it is important to consider the past and present glaciological context of the region and to evaluate any differences in the recorded ice thickness history between nunataks near ice streams and those located in less dynamic areas. For a more comprehensive understanding of ice sheet behaviour, an iterative approach is needed: geological reconstructions need to be investigated using high-resolution numerical models, just as models are evaluated against empirical data.

The EAIS, where grounded below sea level, became increasingly sensitive to ocean warming as basal topography evolved over the past 34 Ma[49]. Thus, there is a real need to adequately capture the interaction of individual ice streams with their subglacial topography in ice sheet models. Our results demonstrate that caution is needed when using AIS responses to past warm climates as analogues for the future because subglacial topography changes significantly on geological time scales. Furthermore, considering the importance of subglacial topography for ice sheet response[38,39,49], there is a clear need to use topographic reconstructions of the target geological period and at a spatial resolution that conforms with high-resolution model domains, thus capturing the complex-terrain influence when modelling ice streams. At present, the available datasets have a resolution of 5 km or coarser, which is not enough to capture local-scale features[39]. It is important to keep in mind that the geophysical relief approach[60] applied to reconstruct the Pliocene topography[61] produces a smooth palaeo topography that does not capture some local features, such as the preserved fluvial valleys beneath Jutulstraumen[36]. For the future, it is important that mechanisms and patterns of glacial erosion are better understood and incorporated in subglacial topographical reconstructions at resolutions that take full advantage of the capabilities of state-of-the-art regional ice sheet models.

The contrasting responses of neighbouring ice streams in western DML under the same warmer-than-present climate scenarios illustrate a stabilising mechanism for runaway grounding-line retreat that has implications across the ice sheet. When a flux gate is wide, a smaller fraction of the ice body is constricted by lateral drag, allowing more ice to flow through (Fig. 9a). As a result, the grounding line becomes more sensitive to the loss of its ice shelf and can retreat more easily. Conversely, narrow flux gates funnel ice from a wider region towards a narrower outlet, creating a bottleneck that provides lateral stresses that are high enough to reduce the outflow of ice and thus decrease mass loss (Fig. 9b). However, as shown by the differences between Jutulstraumen's response to Pliocene vs. modern subglacial topographies, the presence of a deeper trough at the flux gate can outweigh the role played by lateral stresses, increasing the ice stream's susceptibility to dynamic thinning.

A screening of ice streams in East Antarctica reveals that other ice streams might also experience stabilising effects from a narrow flux gate. Assessing whether they act to limit EAIS mass loss or

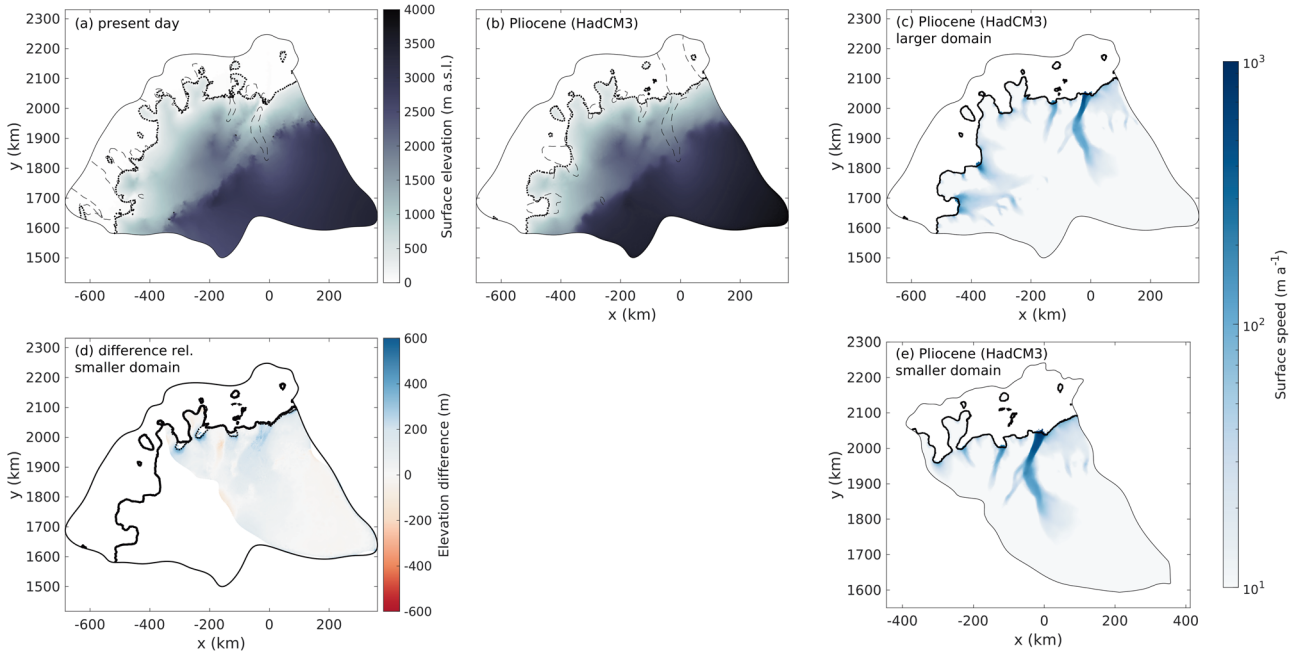

Fig. 4 Showcase of the lower-resolution, larger-domain experiment. a Modern surface topography (m a.s.l.). **b** Pliocene surface topography (the difference between both is presented in Fig. 3a. **c** Pliocene surface speed (ma^{-1}). **d** Pliocene ice-surface elevation difference (m) between the larger-domain and the smaller-domain experiments (blue means the larger domain produces higher elevations). **e** Pliocene surface speed for the smaller domain, for comparison with panel (**c**). Dashed lines in panels **a**, **b** denote the 50 ma^{-1} surface speed contour, while solid lines in all panels show the grounding line. In summary, the larger experiment yields a thicker Jutulstraumen, while Schyttbreen loses less mass due to ice advection from the western part of the domain. This increased mass advection, however, is not enough to significantly counter the effects of dynamic thinning at Schyttbreen or the other smaller glaciers.

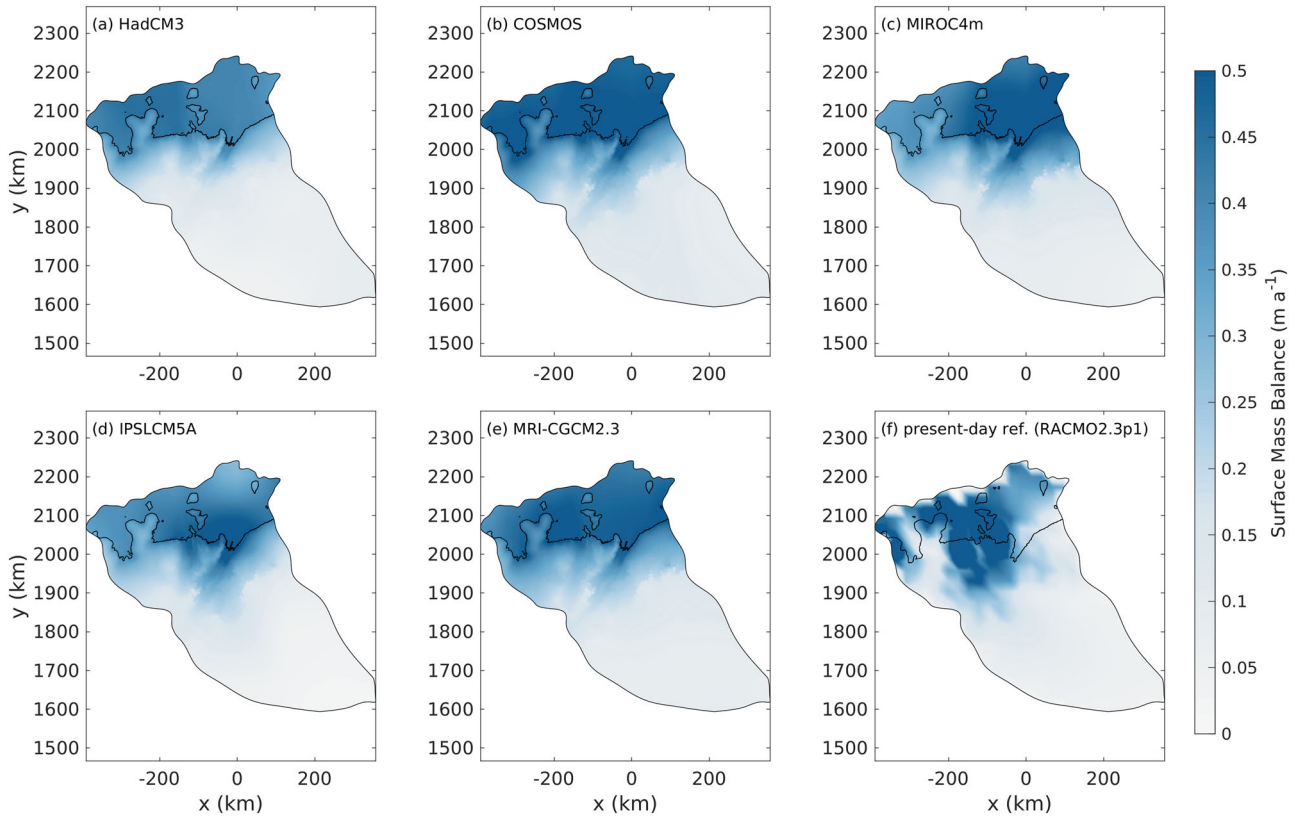

Fig. 5 Surface mass balance based on the different climate models. a–**e** Pliocene surface mass balance (ma^{-1}) computed for all experiments shown in Fig. 2, including lapse-rate corrections. Panel **f** shows the surface mass balance from RACMO2.3p1 in its original form, without corrections for elevation differences. Solid lines in all panels show the present-day grounding line.

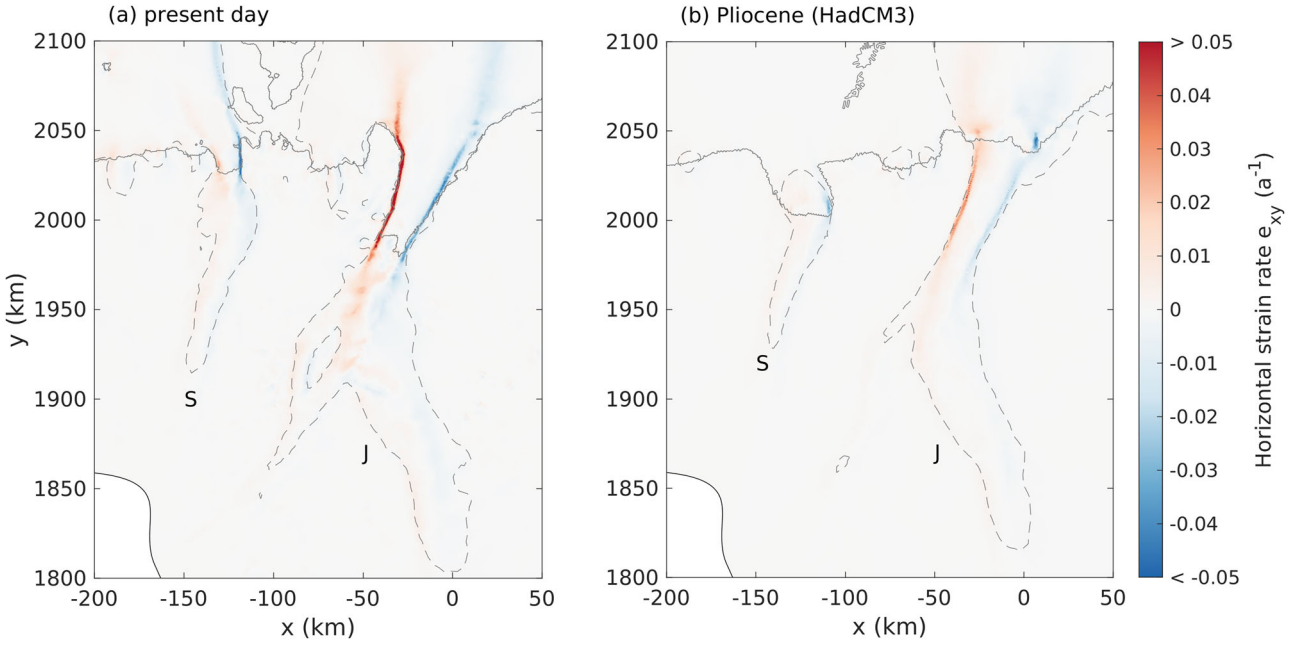

Fig. 6 Lateral stresses are significantly higher along the Jutulstraumen flux gate. Horizontal strain rates (a^{-1}) for **a** the modern ice sheet and **b** the Pliocene ice sheet. The solid line shows the grounding line position and the dashed lines show the 50 ma^{-1} surface speed contour. Schyttbreen and Jutulstraumen are identified by their initials.

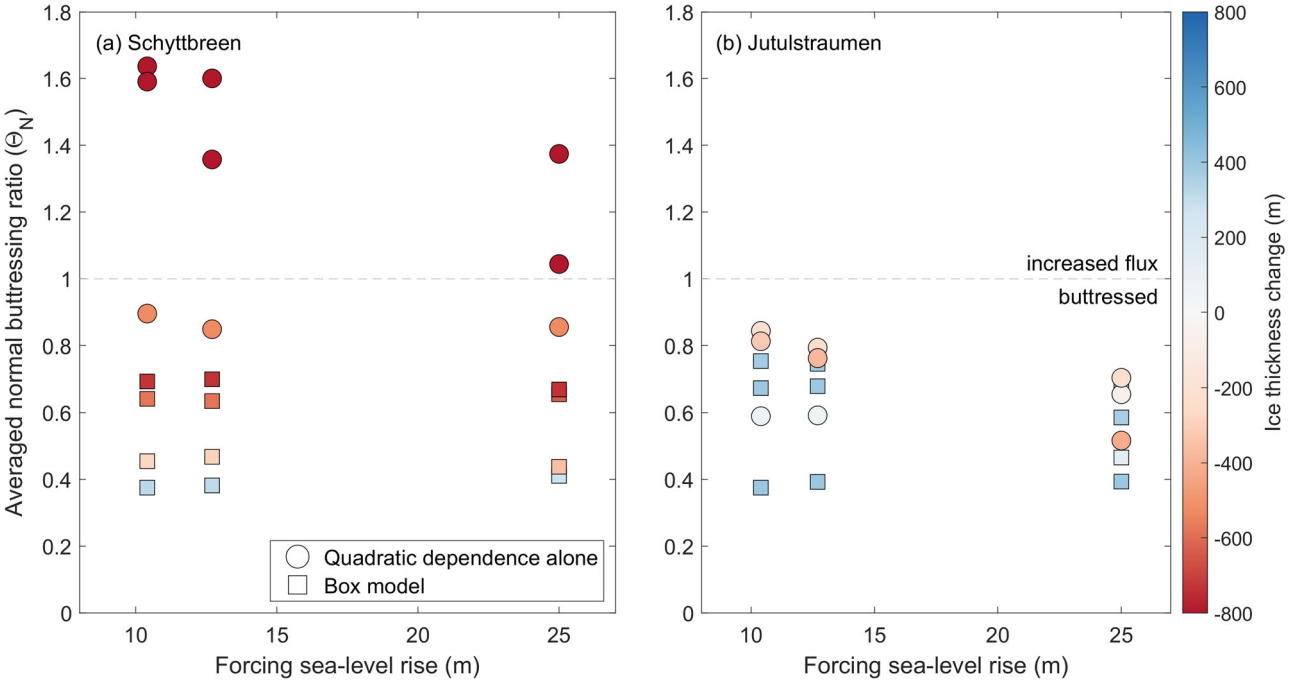

Fig. 7 Ice-shelf buttressing can prevent thinning over Jutulstraumen even under upper-end sea-level rise scenarios. Ice-shelf buttressing and ice thickness change at the modern grounding line for three different sea-level rise and ocean-forcing scenarios over **a** Schyttbreen and **b** Jutulstraumen. Circles mark the experiments where ice-shelf basal melting is prescribed as in the Pliocene experiments but under varying ocean temperatures, while squares mark the experiments where basal melting is obtained from a box model (see Methods). The buttressing ratio[59] quantifies the degree of buttressing provided by an ice shelf at the grounding line compared to the absence of an ice shelf ($\Theta_N < 1$ when buttressing exists, $\Theta_N > 1$ when the stress balance increases ice flux through the grounding line). The number shown is an average along the grounding line for each ice stream (see Fig. 8f), considering the normal stresses. The dashed line highlights the $\Theta_N = 1$ threshold between buttressed and increased-flux conditions.

cause EAIS mass gain, or if they are instead vulnerable to retreat, is necessary for refining our future estimates of sea-level rise. We identify 11 other ice streams in similar topographic settings (i.e., a deep trough and a narrow flux gate; see Methods), of which 9 (10 including Jutulstraumen) are in regions of the EAIS where snowfall is projected to increase[62] (Fig. 10 and Supplementary Table 2). Thus, ice stream thickening under a warmer-than-present climate may not be exclusive to Jutulstraumen, and it remains to be assessed to which extent the narrow flux gates are able to prevent or slow down long-term mass loss from these ice

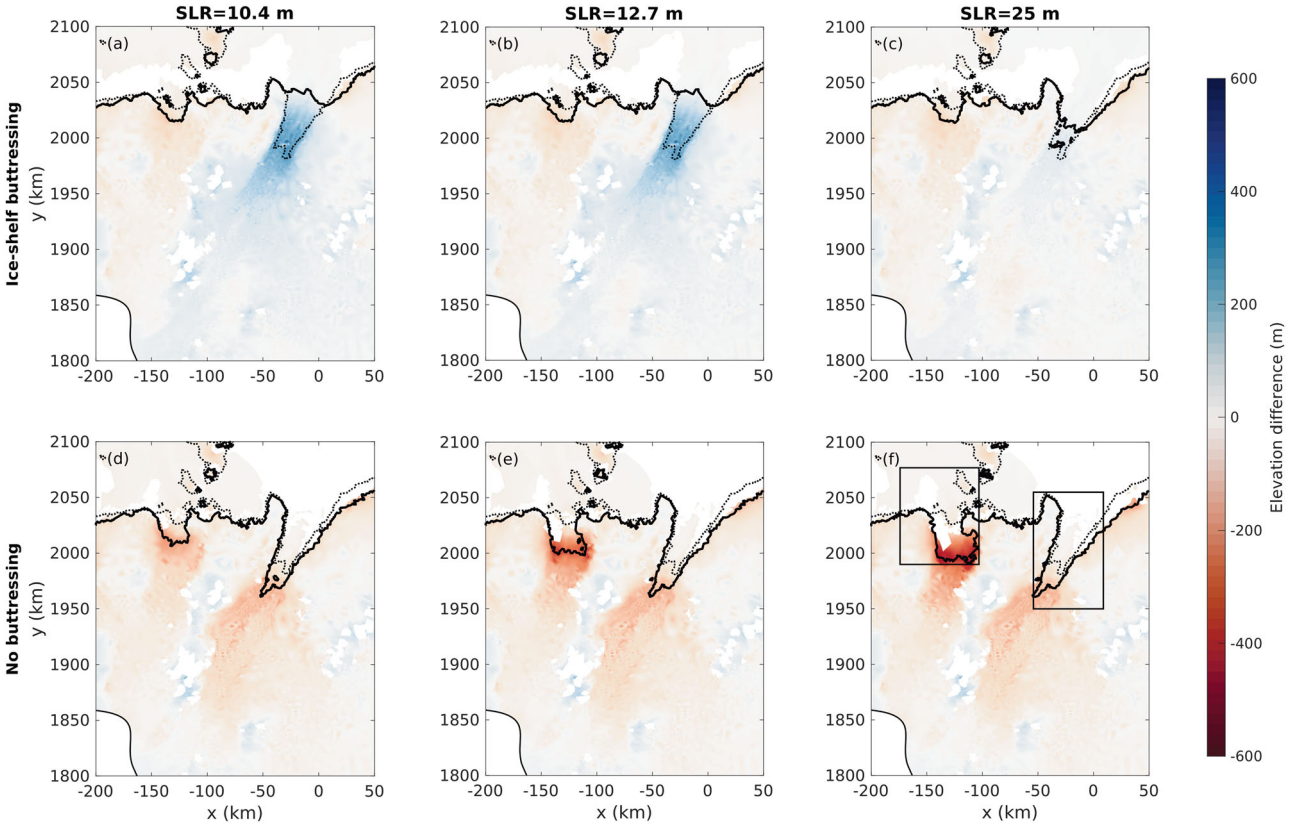

Fig. 8 Ice surface elevation differences between the 1000-year experiments under different sea-level rise scenarios and present day. The upper row **a**–**c** shows the experiments using PICO with an input temperature of −1.0 °C, while the lower row **d**–**f** shows the experiments where the HadCM3 Pliocene ocean forcing was applied. Rectangles in panel **f** show the bounds for computing the buttressing ratio (Fig. 7) over the grounding line for each ice stream. Dashed lines show the modern grounding line, while thick solid lines show the modelled grounding line at the end of the experiment. In short, Jutulstraumen thickens despite sea-level rise as long as its ice shelf provides buttressing.

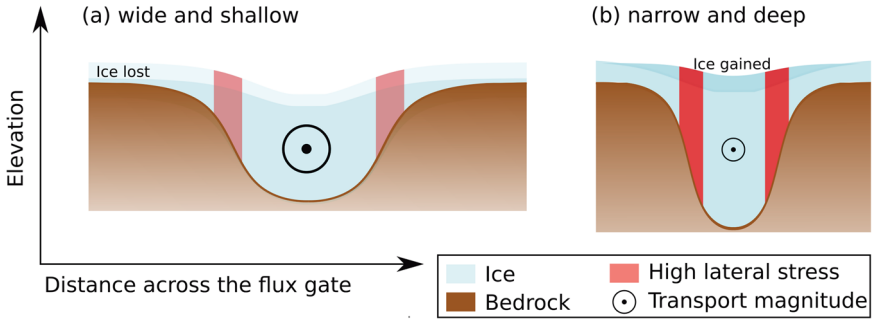

Fig. 9 A narrow flux gate constricts the ice flow due to high lateral stresses. Schematic showing a transect across the flux gate for **a** wide and shallow troughs (e.g., Schyttbreen) and **b** narrow and deep troughs (e.g., Jutulstraumen). High lateral stresses are highlighted in red, while the ice flow is represented as a vector pointing out of the page. Ice-flow constriction can lead to ice stream thickening as less mass is transported towards the ice shelf. Conversely, a wide and shallow flux gate allows more mass loss and, thus, ice sheet thinning under reduced ice-shelf buttressing. Although these are flux gate cross-sectional representations, it is worth reminding that these stresses act along considerable distances upstream (Fig. 6).

streams in a future warmer world. Together, these 10 basins account for 27% of the EAIS in both area and discharge[63]. A careful evaluation is required of the response of these critical ice streams using basin-scale, high-resolution numerical models. At least half of these ice streams have been previously identified as of high interest to determine the EAIS future[24]. Thus, more accurate assessments of the interplay between lateral drag, ice-shelf buttressing, and marine ice sheet instability will improve our estimates of EAIS sensitivity to grounding-line retreat and its potential future contributions to sea-level rise.

As in atmosphere and ocean models, the artificial smoothing of topography due to low spatial resolution prevents coarse-resolution ice sheet models from properly capturing regional topographically controlled dynamics[37–39]. In the case of ice sheet models, the inclusion of over-deepened subglacial topographies is key for a proper assessment of whether marine ice sheet instability might trigger runaway retreat of the grounding line in a retrograde bed slope ice stream[24]. We show here that a proper representation of subglacial topography is critical to assessing an ice stream's response to climate change and that geological

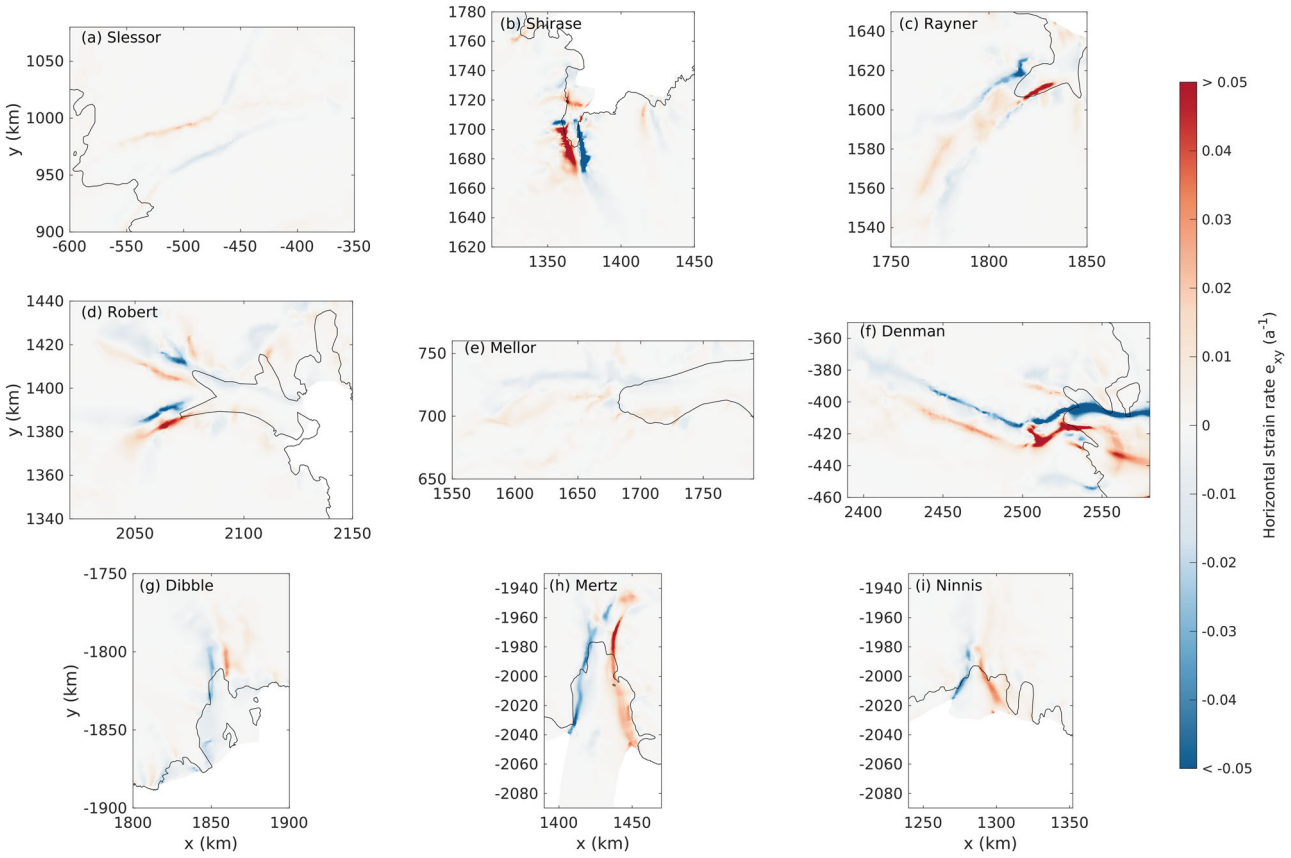

Fig. 10 Horizontal strain rates (a^{-1}) for each identified ice stream in a similar topographic setting to Jutulstraumen along the EAIS margin. a Slessor, **b** Shirase, **c** Rayner, **d** Robert, **e** Mellor, **f** Denman, **g** Dibble, **h** Mertz, and **i** Ninnis glaciers. Ice streams identified from high lateral stresses[58], and over which precipitation is projected to increase[62]. Solid lines show the modern grounding line. Locations of these ice streams are shown in Supplementary Fig. 6.

reconstructions might not accurately reflect the future response of an ice stream. The potential for dynamic thinning and corresponding contribution to sea-level rise is dependent on whether the ice stream flux gate geometry is narrow and shallow/deep or wide and shallow/deep. For Jutulstraumen, a combination of increasing inland snowfall under warming conditions[26,57], a subglacial topography that funnels much of this excess ice through a constricting flux gate, and significant ice-shelf buttressing can explain the trend of mass gain[32]. Nine additional ice streams along the EAIS margin present this complex combination of conditions and need to be more thoroughly assessed regarding how they interact with (i) the bounding topography, (ii) a warmer ocean, and (iii) increased snow accumulation conditions characteristic of a warmer climate. This will ultimately improve estimates of future EAIS mass change, highlighting whether the EAIS is able to offset the mass loss from the West Antarctic and Greenland ice sheets and lead to refined uncertainties in global sea-level projections. Because ice shelves are the key components determining whether a switch from ice stream thickening to ice stream thinning could send Antarctica into irreversible retreat, it is most pertinent that we understand and closely monitor their health and stability.

Methods

Ice sheet model. All simulations were performed using the ice-flow model Úa[41], which has been used previously for palaeo-time scale simulations[39,53]. We model the Jutulstraumen catchment, as defined in ref. [64] for the grounded part, but extend the domain to the continental shelf break. The model solves the shallow shelf approximation of the Stokes equations using the finite-element method over an irregular mesh. The mesh resolution is 10 km over the less dynamic areas of the domain and is refined to ca. 500 m over regions of steep subglacial topography and at grounding zones. The latter is defined as the area within 2 km of where ice becomes afloat. In the larger-domain simulation (presented in Section "Contrasting responses between ice streams during the Pliocene"), the mesh is refined to only 1 km within 4 km on either side of the grounding line. In all experiments, the mesh is updated during simulation time (every 20 model years) to track and maintain a high resolution over these targeted features as the ice sheet geometry evolves.

The thermal state of the ice sheet is not explicitly solved and is instead implicitly accounted for in the strain-rate coefficient (A) of Glen's Flow Law (using $n = 3$). A distribution of A is obtained, together with a distribution of basal sliding coefficients (C), through an inversion procedure (Supplementary Fig. 3). For this procedure, we use modern ice surface velocities from MEaSUREs[65] and modern bedrock topography from BedMachine–Antarctica[23], including the most up-to-date data for Jutulstraumen[36]. The distribution of basal sliding coefficients is used in conjunction with Weertman's sliding law (using $m = 3$; an assessment of this choice is presented in Supplementary Note 2). Following recent studies[66], we add an extra term in the inversion procedure to penalise changes in ice thickness, which minimises model drift at the start of time-dependent runs. Our model setup leads to a well-resolved ice flow of all modern ice streams and minor glaciers within the simulated catchment and,

therefore, realistically captures the glacial dynamics of western DML. Although our inverted fields are not fully consistent with the reconstructed Pliocene topography, since they use modern conditions as input, there are no ice-surface velocity data available to carry out a similar procedure for the Pliocene, nor sufficiently available geological constraints to reliably estimate a spatial distribution of C based on other procedures (e.g., ref. [67]). This limitation is not exclusive to our model or choice of how to prescribe basal sliding, but a general characteristic of palaeo ice sheet models[67–69]. We note, however, that ice rheological features, such as a weakening of the ice stream margins due to shear heating, are captured in the spatial distribution of A (Supplementary Fig. 3a). Nevertheless, we perform sensitivity tests to an overall ice warming and a further weakened ice margin, which would reduce lateral stresses at the margins of Jutulstraumen (Supplementary Note 1).

Finally, ice-shelf basal melting is computed assuming a quadratic local dependence on ocean temperature[70], and calving is prescribed as a thickness threshold based on modern ice-shelf thicknesses, where ice thinner than 200 m is instantly calved away[71]. Due to numerical considerations, in finite-element models such as Úa, the "de facto" calving front is located at the downstream end of the domain, with a thin layer of inactive ice at the prescribed minimum thickness (10 m) covering the area between what we consider the calving front and the downstream domain boundary. Recent studies using one-dimensional steady-state models have shown that how the calving front is treated in ice-sheet models has an impact on ice flux through the grounding line, which could be larger than ice-shelf melting[9,12] and could have influenced our results. How these findings apply to time-dependent ice flow simulations along two horizontal dimensions, however, remains to be assessed.

Pliocene model forcings. We simulate equilibrium ice geometries of Jutulstraumen's catchment under Pliocene climate conditions derived from a subset of five climate models from the Pliocene Model Intercomparison Project Phase 1[42–46] (Supplementary Table 3), which includes the control simulation used in the PLISMIP-ANT project[25]. Pliocene surface mass balance is computed as accumulation minus ablation, which are calculated from the respective climate model's monthly climatology of near-surface atmospheric temperature and precipitation. Both fields are corrected for the mismatch between the topographies from the climate model and our ice-flow model through lapse rates of $-8\,°C\,km^{-1}$[72] and 7% $°C^{-1}$[73] for temperature and precipitation, respectively. Accumulation is computed as the fraction of solid precipitation based on surface atmospheric temperature[74], and ablation is computed through a semi-analytical solution of the positive degree-day model[75]. We evolve the surface mass balance linearly over 1000 years to ensure a smooth transition from modern to Pliocene conditions. Surface mass balance starts from modern RACMO2.3p1[76] and evolves to the Pliocene distribution as described above, applying a topographic lapse-rate correction each time the model mesh is updated. Sea level, conversely, is set to 25 m above present from the start of each experiment, as in PLISMIP-ANT[72]. Ocean temperatures are also constant and applied uniformly under the ice shelves. They are computed from the respective climate models as the 400 m-depth average over the region offshore from our modelled domain's grounding line (i.e., between $y = 1950$ and $y = 2300$ km and between $x = -400$ and $x = 200$ km following the EPSG3031 projection). Although our model does not include an interactive evolving lithosphere, we performed experiments using the three available mid-Pliocene bed topography reconstructions[48]. The impact of the different bed topographies and initial conditions on the resulting ice sheet configurations was much smaller than the changes observed in the main experiments (Supplementary Note 3). Furthermore, a wide range of glacial isostatic adjustment models shows the lithosphere response over the modelled region to be small and uniform, at least since the last deglaciation[77]. We further note that the Pliocene topographies used in this study are reconstructed using the geophysical relief approach[60] whereby offshore Pliocene-present sediment volumes are loaded in onshore depressions up to a 'summit accordance surface' created by interpolating between the highest summits defined within a circular sliding window of 30 km radius[48]. This approach is designed to capture key trends in landscape evolution but is likely to create an unrealistically smooth paleo-landscape[48]. Since an artificially smooth Pliocene topography may lead to overestimated basal sliding rates, we test a scenario where sliding rates are kept at a uniform low rate of $10\,m\,a^{-1}$, representative of the least dynamic areas of the ice sheet (Supplementary Note 2 and Supplementary Fig. 2a).

Simulations start from the modern BedMachine-Antarctica ice surface elevation[23] as opposed to ice thickness to avoid geometry inconsistencies from using a significantly different subglacial topography. An experiment was also performed starting from the PRISM4 reconstructed Pliocene surface topography[4], which showed an equilibrium geometry close to that starting from the modern ice surface (Supplementary Fig. 5). Nevertheless, we opted for the modern surface topography as our starting conditions for a consistent comparison with the present-day ice surface. All experiments are run until they are in close equilibrium with the forcing climate, which we consider when their total ice volume changes less than ca. 0.5% over five thousand model years. This state is achieved after twenty to thirty thousand model years, depending on the experiment. All Pliocene sensitivity tests were performed using HadCM3 as the forcing climate model. The modern reference ice sheet geometry used in all comparisons is a relaxation run of 10 and 100 years for the higher and lower resolution experiments, respectively, under their respective initial conditions. The lower resolution experiment is also performed using HadCM3 as the forcing climate, and the main differences between both domains are summarised in Fig. 4.

Response of the modern ice sheet to future-like ocean scenarios. We perform a total of twenty-one 1000-year experiments, which all start from the modern BedMachine-Antarctica ice sheet geometry, inverted A and C fields, and use constant RACMO2.3p1 surface mass balance[76]. These experiments are a combination of seven different ice-shelf melting scenarios using two distinct parameterisations for basal melting and three different sea-level rise scenarios. The first set of ice-shelf basal melting scenarios uses the same parameterisation as in the Pliocene experiments. Within this set, one scenario uses ocean temperatures derived from the modern ocean temperatures in the World Ocean Atlas 2018 (0.05 °C)[78]. Another scenario uses the Pliocene HadCM3 ocean temperatures (1.60 °C), and the third assumes an extreme scenario of 2.00 °C. The latter two are able to greatly reduce the extent of all ice shelves over the simulation period (see Fig. 8d–f for the 1.60 °C case). The second set of ice-shelf basal melting parameterisations uses the PICO box model[79] to mimic the overturning circulation under modern ice-shelf cavities. We use four fixed values for its input temperature ([−1.6, −1.4, −1.2, −1.0] °C). This range has as a lower boundary the value used for the Jutulstraumen basin in a continental-scale experiment using PICO[79,80] and as an upper boundary the closest value that prevents unrealistic grounding-line advance from Schyttbreen under modern climate conditions and sea level. For each of these seven ice-shelf basal melting scenarios, we perform

three experiments that reflect different upper-boundary estimates of global sea-level rise, as determining local sea-level changes is not trivial[81]. Sea level is linearly raised over the first 300 model years from present day by a total of 10.4, 12.7, and 25.0 m. The first value is based on the high-end estimate of sea-level rise for the most pessimistic IPCC scenario by 2300[82], the second reflects a full contribution from Greenland and the WAIS to sea-level rise[23], and the third is the same value used in the Pliocene (and PLISMIP) experiments[72]. After the first 300 years, we keep the forcings constant until the simulation reaches 1000 years of model time. These experiments are summarised in Supplementary Table 1.

Identifying topographically constrained EAIS ice streams. We use results from a present-day Antarctic-wide simulation[58] performed with the same ice sheet model to identify ice streams along the EAIS margin that are in a similar topographic setting to Jutulstraumen and present higher lateral stresses at their flux gates than at their surroundings, also extending further upstream. From this subset, we only account for those that also present a narrow flux gate, i.e., where the grounding line forms an embayment and the ice stream trunk is deeper than its surroundings, showing signs of over-deepening through time. We are able to identify 11 ice streams, in addition to Jutulstraumen, that follow such criteria. Out of these 11 ice streams, 9 are located in regions where precipitation is projected to increase, as is the case for Jutulstraumen[62]. For each of the 11 ice streams, we summarise in Supplementary Table 2 whether they show any changes in surface elevation at their flux gates[83], in mass balance over their respective basins[32], and in projected changes in precipitation over their grounded area by 2100 according to CMIP5 and CMIP6 models[62].

Data availability

The ITS_LIVE data is available at https://doi.org/10.5067/6II6VW8LLWJ7. The MEaSUREs ice velocity data set for Antarctica is available at https://doi.org/10.5067/MEASURES/CRYOSPHERE/nsidc-0484.001. The original BedMachine-Antarctica dataset is available at https://doi.org/10.5067/C2GFER6PTOS4. The updated Jutulstraumen thickness estimates are available at https://doi.org/10.1594/PANGAEA.911475. Reconstructed Pliocene topographies are available at https://doi.org/10.1594/PANGAEA.923109. PRISM4 surface topography is available at https://geology.er.usgs.gov/egpsc/prism/4_data.html. RACMO2.3p1 and model outputs from the Pliocene Model Intercomparison Project are available upon request to the authors of the original publications (refs. [76] and [47] respectively).

Code availability

A version of the record for Úa's source code is available at https://doi.org/10.5281/zenodo.3706624, and the current version is available at https://github.com/GHilmarG/UaSource. Model configuration files to reproduce the experiments shown are available at https://doi.org/10.5281/zenodo.8228879.

Received: 10 October 2022; Accepted: 30 August 2023;
Published online: 11 September 2023

References

1. Gulev, S. et al. Changing State of the Climate System (eds Masson-Delmotte, V. et al.) in *Climate Change 2021: The Physical Science Basis. Contribution of Working Group I to the Sixth Assessment Report of the Intergovernmental Panel on Climate Change* 287–422 (Cambridge University Press, Cambridge, United Kingdom, and New York, NY, USA, 2021).
2. Naish, T. et al. Obliquity-paced Pliocene West Antarctic ice sheet oscillations. *Nature* **458**, 322–328 (2009).
3. Reinardy, B. T. I. et al. Repeated advance and retreat of the East Antarctic Ice Sheet on the continental shelf during the early Pliocene warm period. *Palaeogeogr. Palaeoclimatol. Palaeoecol.* **422**, 65–84 (2015).
4. Dowsett, H. et al. The PRISM4 (mid-Piacenzian) paleoenvironmental reconstruction. *Climate* **12**, 1519–1538 (2016).
5. Bertram, R. A. et al. Pliocene deglacial event timelines and the biogeochemical response offshore Wilkes Subglacial Basin, East Antarctica. *Earth Planet. Sci. Lett.* **494**, 109–116 (2018).
6. Dutton, A. et al. Sea-level rise due to polar ice-sheet mass loss during past warm periods. *Science* **349**, aaa4019 (2015).
7. Grant, G. R. et al. The amplitude and origin of sea-level variability during the Pliocene epoch. *Nature* **574**, 237–241 (2019).
8. Fox-Kemper, B. et al. *Ocean, cryosphere and sea level change.* (eds Masson-Delmotte, V. et al.) in *Climate Change 2021: The Physical Science Basis. Contribution of Working Group I to the Sixth Assessment Report of the Intergovernmental Panel on Climate Change* 1211–1362 (Cambridge University Press, Cambridge, United Kingdom, and New York, NY, USA, 2021).
9. Haseloff, M. & Sergienko, O. V. The effect of buttressing on grounding line dynamics. *J. Glaciol.* **64**, 417–431 (2018).
10. Reese, R., Albrecht, T., Mengel, M., Asay-Davis, X. & Winkelmann, R. Antarctic sub-shelf melt rates via PICO. *Cryosphere* **12**, 1969–1985 (2018).
11. Shepherd, A. et al. Mass balance of the Antarctic Ice Sheet from 1992 to 2017. *Nature* **558**, 219–222 (2018).
12. Haseloff, M. & Sergienko, O. V. Effects of calving and submarine melting on steady states and stability of buttressed marine ice sheets. *J. Glaciol.* **68**, 1149–1166 (2022).
13. Dupont, T. K. & Alley, R. B. Assessment of the importance of ice-shelf buttressing to ice-sheet flow. *Geophys. Res. Lett.* **32**, L04503 (2005).
14. Schoof, C. Ice sheet grounding line dynamics: steady states, stability, and hysteresis. *J. Geophys. Res.* **112**, F03S28 (2007).
15. Gudmundsson, G. H., Krug, J., Durand, G., Favier, L. & Gagliardini, O. The stability of grounding lines on retrograde slopes. *Cryosphere* **6**, 1497–1505 (2012).
16. Barletta, V. R. et al. Observed rapid bedrock uplift in Amundsen Sea Embayment promotes ice-sheet stability. *Science* **360**, 1335–1339 (2018).
17. Robel, A. A., Pegler, S. S., Catania, G., Felikson, D. & Simkins, L. M. Ambiguous stability of glaciers at bed peaks. *J. Glaciol.* **68**, 1177–1184 (2022).
18. Sergienko, O. V. & Wingham, D. J. Bed topography and marine ice-sheet stability. *J. Glaciol.* **68**, 124–138 (2022).
19. Jamieson, S. S. R. et al. Ice-stream stability on a reverse bed slope. *Nat. Geosci.* **5**, 799–802 (2012).
20. Favier, L. et al. Retreat of Pine Island Glacier controlled by marine ice-sheet instability. *Nat. Clim. Change* **4**, 117–121 (2014).
21. Rignot, E., Mouginot, J., Morlighem, M., Seroussi, H. & Scheuchl, B. Widespread, rapid grounding line retreat of Pine Island, Thwaites, Smith, and Kohler glaciers, West Antarctica, from 1992 to 2011. *Geophys. Res. Lett.* **41**, 3502–3509 (2014).
22. Kimura, S. et al. Oceanographic controls on the variability of ice-shelf basal melting and circulation of glacial meltwater in the Amundsen Sea Embayment, Antarctica. *J. Geophys. Res.* **122**, 10131–10155 (2017).
23. Morlighem, M. et al. Deep glacial troughs and stabilizing ridges unveiled beneath the margins of the Antarctic ice sheet. *Nat. Geosci.* **13**, 132–137 (2020).
24. Stokes, C. R. et al. Response of the East Antarctic Ice Sheet to past and future climate change. *Nature* **608**, 275–286 (2022).
25. de Boer, B. et al. Simulating the Antarctic ice sheet in the late-Pliocene warm period: PLISMIP-ANT, an ice-sheet model intercomparison project. *Cryosphere* **9**, 881–903 (2015).
26. Frieler, K. et al. Consistent evidence of increasing Antarctic accumulation with warming. *Nat. Clim. Change* **5**, 348–352 (2015).
27. Yamane, M. et al. Exposure age and ice-sheet model constraints on Pliocene East Antarctic ice sheet dynamics. *Nat. Commun.* **6**, 7016 (2015).
28. Rhee, H. H. et al. Quaternary ice thinning of David Glacier in the Terra Nova Bay region, Antarctica. *Quat. Geochronol.* **67**, 101233 (2022).
29. Pollard, D. & DeConto, R. M. Modelling West Antarctic ice sheet growth and collapse through the past five million years. *Nature* **458**, 329–332 (2009).
30. Jones, R. S. et al. Cosmogenic nuclides constrain surface fluctuations of an East Antarctic outlet glacier since the Pliocene. *Earth Planet. Sci. Lett.* **480**, 75–86 (2017).
31. Edwards, T. L. et al. Projected land ice contributions to twenty-first-century sea level rise. *Nature* **593**, 74–82 (2021).
32. Velicogna, I. et al. Continuity of ice sheet mass loss in Greenland and Antarctica from the GRACE and GRACE Follow-On missions. *Geophys. Res. Lett.* **47**, e2020GL087291 (2020).
33. Prentice, M. L. & Matthews, R. K. Tertiary ice sheet dynamics: the snow gun hypothesis. *J. Geophys. Res.* **96**, 6811–6827 (1991).
34. Parrenin, F. et al. 1-D-ice flow modelling at EPICA Dome C and Dome Fuji, East Antarctica. *Climate* **3**, 243–259 (2007).
35. Suganuma, Y., Miura, H., Zondervan, A. & Okuno, J. East Antarctic deglaciation and the link to global cooling during the Quaternary: evidence

from glacial geomorphology and ^{10}Be surface exposure dating of the Sør Rondane Mountains, Dronning Maud Land. *Quat. Sci. Rev.* **97**, 102–120 (2014).
36. Franke, S. et al. Preserved landscapes underneath the Antarctic Ice Sheet reveal the geomorphological history of Jutulstraumen Basin. *Earth Surf. Process. Landf.* **46**, 2728–2745 (2021).
37. Durand, G., Gagliardini, O., Favier, L., Zwinger, T. & le Meur, E. Impact of bedrock description on modeling ice sheet dynamics. *Geophys. Res. Lett.* **38**, L20501 (2011).
38. Cuzzone, J. K. et al. The impact of model resolution on the simulated Holocene retreat of the southwestern Greenland ice sheet using the Ice Sheet System Model (ISSM). *Cryosphere* **13**, 879–893 (2019).
39. Mas e Braga, M. et al. Nunataks as barriers to ice flow: implications for palaeo ice sheet reconstructions. *Cryosphere* **15**, 4929–4947 (2021).
40. Stutz, J. et al. Mid-Holocene thinning of David Glacier, Antarctica: chronology and controls. *Cryosphere* **15**, 5447–5471 (2021).
41. Gudmundsson, H. GHilmarG/UaSource: Ua2019b. *Zenodo* (2020).
42. Bragg, F. J., Lunt, D. J. & Haywood, A. M. Mid-Pliocene climate modelled using the UK Hadley Centre Model: PlioMIP Experiments 1 and 2. *Geosci. Model Dev.* **5**, 1109–1125 (2012).
43. Stepanek, C. & Lohmann, G. Modelling mid-Pliocene climate with COSMOS. *Geosci. Model Dev.* **5**, 1221–1243 (2012).
44. Contoux, C., Ramstein, G. & Jost, A. Modelling the mid-Pliocene Warm Period climate with the IPSL coupled model and its atmospheric component LMDZ5A. *Geosci. Model Dev.* **5**, 903–917 (2012).
45. Chan, W.-L., Abe-Ouchi, A. & Ohgaito, R. Simulating the mid-Pliocene climate with the MIROC general circulation model: Experimental design and initial results. *Geosci. Model Dev.* **4**, 1035–1049 (2011).
46. Kamae, Y. & Ueda, H. Mid-Pliocene global climate simulation with MRI-CGCM2.3: Set-up and initial results of PlioMIP Experiments 1 and 2. *Geosci. Model Dev.* **5**, 793–808 (2012).
47. Dolan, A. M., De Boer, B., Bernales, J., Hill, D. J. & Haywood, A. M. High climate model dependency of Pliocene Antarctic ice-sheet predictions. *Nat. Commun.* **9**, 2799 (2018).
48. Paxman, G. J. G. et al. Reconstructions of Antarctic topography since the Eocene–Oligocene boundary. *Palaeogeogr. Palaeoclimatol. Palaeoecol.* **535**, 109346 (2019).
49. Paxman, G. J. G., Gasson, E. G. W., Jamieson, S. S. R., Bentley, M. J. & Ferraccioli, F. Long-term increase in Antarctic Ice Sheet vulnerability driven by bed topography evolution. *Geophys. Res. Lett.* **47**, e2020GL090003 (2020).
50. Humbert, A. & Steinhage, D. The evolution of the western rift area of the Fimbul Ice Shelf, Antarctica. *Cryosphere* **5**, 931–944 (2011).
51. Høydal, Ø. A. A force-balance study of ice flow and basal conditions of Jutulstraumen, Antarctica. *J. Glaciol.* **42**, 413–425 (1996).
52. Suckale, J., Platt, J. D., Perol, T. & Rice, J. R. Deformation-induced melting in the margins of the West Antarctic ice streams. *J. Geophys. Res.* **119**, 1004–1025 (2014).
53. Jones, R. S., Gudmundsson, G. H., Mackintosh, A. N., McCormack, F. S. & Whitmore, R. J. Ocean-driven and topography-controlled nonlinear glacier retreat during the Holocene: Southwestern Ross Sea, Antarctica. *Geophys. Res. Lett.* **48**, e2020GL091454 (2021).
54. Becquey, S. & Gersonde, R. Past hydrographic and climatic changes in the Subantarctic Zone of the South Atlantic – The Pleistocene record from ODP Site 1090. *Palaeogeogr. Palaeoclimatol. Palaeoecol.* **182**, 221–239 (2002).
55. Stenni, B. et al. The deuterium excess records of EPICA Dome C and Dronning Maud Land ice cores (East Antarctica). *Quat. Sci. Rev.* **29**, 146–159 (2010).
56. Huybrechts, P., Rybak, O., Steinhage, D. & Pattyn, F. Past and present accumulation rate reconstruction along the Dome Fuji–Kohnen radio-echo sounding profile, Dronning Maud Land, East Antarctica. *Ann. Glaciol.* **50**, 112–120 (2009).
57. Altnau, S., Schlosser, E., Isaksson, E. & Divine, D. Climatic signals from 76 shallow firn cores in Dronning Maud Land, East Antarctica. *Cryosphere* **9**, 925–944 (2015).
58. Gudmundsson, G. H., Paolo, F. S., Adusumilli, S. & Fricker, H. A. Instantaneous Antarctic ice sheet mass loss driven by thinning ice shelves. *Geophys. Res. Lett.* **46**, 13903–13909 (2019).
59. Gudmundsson, H. Ice-shelf buttressing and the stability of marine ice sheets. *Cryosphere* **7**, 647–655 (2013).
60. Small, E. E. & Anderson, R. S. Pleistocene relief production in Laramide mountain ranges, western United States. *Geology* **26**, 123 (1998).
61. Paxman, G. J. G. et al. Uplift and tilting of the Shackleton Range in East Antarctica driven by glacial erosion and normal faulting. *J. Geophys. Res.* **122**, 2390–2408 (2017).
62. Tewari, K., Mishra, S. K., Salunke, P. & Dewan, A. Future projections of temperature and precipitation for Antarctica. *Environ. Res. Lett.* **17**, 014029 (2022).
63. Rignot, E. et al. Four decades of Antarctic Ice Sheet mass balance from 1979–2017. *Proc. Natl Acad. Sci. USA* **116**, 1095–1103 (2019).
64. Zwally, H. J., Giovinetto, M. B., Beckley, M. A. & Saba, J. L. Antarctic and Greenland drainage systems. GSFC Cryospheric Sciences Laboratory. http://icesat4.gsfc.nasa.gov/cryo_data/ant_grn_drainage_systems.php (2012).
65. Rignot, E., Mouginot, J. & Scheuchl, B. Ice flow of the Antarctic Ice Sheet. *Science* **333**, 1427–1430 (2011).
66. Rosier, S. H. R. et al. The tipping points and early warning indicators for Pine Island Glacier, West Antarctica. *Cryosphere* **15**, 1501–1516 (2021).
67. Pollard, D. & DeConto, R. M. A simple inverse method for the distribution of basal sliding coefficients under ice sheets, applied to Antarctica. *Cryosphere* **6**, 953–971 (2012).
68. Martin, M. A. et al. The Potsdam Parallel Ice Sheet Model (PISM-PIK)—Part 2: dynamic equilibrium simulation of the Antarctic ice sheet. *Cryosphere* **5**, 727–740 (2011).
69. Albrecht, T., Winkelmann, R. & Levermann, A. Glacial-cycle simulations of the Antarctic Ice Sheet with the Parallel Ice Sheet Model (PISM)—Part 2: parameter ensemble analysis. *Cryosphere* **14**, 633–656 (2020).
70. Favier, L. et al. Assessment of sub-shelf melting parameterisations using the ocean–ice-sheet coupled model NEMO (v3. 6)–Elmer/Ice (v8. 3). *Geosci. Model Dev.* **12**, 2255–2283 (2019).
71. DeConto, R. M. & Pollard, D. Contribution of Antarctica to past and future sea-level rise. *Nature* **531**, 591–597 (2016).
72. Dolan, A. M., Koenig, S. J., Hill, D. J., Haywood, A. M. & DeConto, R. M. Pliocene Ice Sheet Modelling Intercomparison Project (PLISMIP)—experimental design. *Geosci. Model Dev.* **5**, 963–974 (2012).
73. Albrecht, T., Winkelmann, R. & Levermann, A. Glacial-cycle simulations of the Antarctic Ice Sheet with the Parallel Ice Sheet Model (PISM)—Part 1: boundary conditions and climatic forcing. *Cryosphere* **14**, 599–632 (2020).
74. Marsiat, I. Simulation of the Northern Hemisphere continental ice sheets over the last glacial-interglacial cycle: Experiments with a latitude-longitude vertically integrated ice sheet model coupled to a zonally averaged climate model. *Palaeoclimates* **1**, 59–98 (1994).
75. Calov, R. & Greve, R. A semi-analytical solution for the positive degree-day model with stochastic temperature variations. *J. Glaciol.* **51**, 173–175 (2005).
76. Wessem, J. M. V. et al. Improved representation of East Antarctic surface mass balance in a regional atmospheric climate model. *J. Glaciol.* **60**, 761–770 (2014).
77. Whitehouse, P. L., Gomez, N., King, M. A. & Wiens, D. A. Solid Earth change and the evolution of the Antarctic Ice Sheet. *Nat. Commun.* **10**, 503 (2019).
78. Locarnini, M. et al. World Ocean Atlas 2018, volume 1: temperature. *NOAA Atlas NESDIS* **81**, 52pp (2018).
79. Reese, R., Winkelmann, R. & Gudmundsson, G. H. Grounding-line flux formula applied as a flux condition in numerical simulations fails for buttressed Antarctic ice streams. *Cryosphere* **12**, 3229–3242 (2018).
80. Schmidtko, S., Heywood, K. J., Thompson, A. F. & Aoki, S. Multidecadal warming of Antarctic waters. *Science* **346**, 1227–1231 (2014).
81. Gomez, N., Weber, M. E., Clark, P. U., Mitrovica, J. X. & Han, H. K. Antarctic ice dynamics amplified by Northern Hemisphere sea-level forcing. *Nature* **587**, 600–604 (2020).
82. van de Wal, R. S. W. et al. A high-end estimate of sea-level rise for practitioners. *Earth and Space Science Open Archive* https://doi.org/10.1002/essoar.10510742.1 (2022).
83. Shepherd, A., Fricker, H. A. & Farrell, S. L. Trends and connections across the Antarctic cryosphere. *Nature* **558**, 223–232 (2018).
84. Gardner, A. S. et al. Increased West Antarctic and unchanged East Antarctic ice discharge over the last 7 years. *Cryosphere* **12**, 521–547 (2018).

Acknowledgements

This work is supported by Stockholm University (APS), Norwegian Polar Institute/NARE under Grant "MAGIC-DML" (OF), the US National Science Foundation under Grant No. OPP-1542930 (NAL and JMH), Swedish Research Council under Grant No. 2016-04422 (JMH and APS), and the German Research Foundation Priority Programme 1158 "Antarctic Research" under Grant No. 365737614 (IR and Matthias Prange). R.S.J. is supported by the Australian Research Council under grants DE210101923 and SR200100005 (Securing Antarctica's Environmental Future). The computations and data handling were enabled by resources provided by the Swedish National Infrastructure for Computing (SNIC) at the National Supercomputer Centre (NSC), partially funded by the Swedish Research Council through grant agreement No. 2018-05973.

Author contributions

M.M.B. idealised and designed the study, with close input from R.S.J., J.B., J.L.A., I.R., and A.P.S. M.M. provided the BedMachine-Antarctica data set using the updated Jutulstraumen topography. M.M.B. performed all simulations and analysed the results. M.M.B. wrote the paper with input from R.S.J., J.B., J.L.A., O.F., M.M., A.J.K., N.A.L., J.M.H., Y.S., N.F.G., I.R., and A.P.S.

Funding

Open access funding provided by Stockholm University.

Competing interests
The authors declare no competing interests.

Additional information
Supplementary information The online version contains supplementary material available at https://doi.org/10.1038/s43247-023-00983-3.

Correspondence and requests for materials should be addressed to Martim Mas e Braga.

Peer review information *Communications Earth & Environment* thanks Sandra Passchier and the other anonymous reviewer(s) for their contribution to the peer review of this work. Primary Handling Editors: Christophe Kinnard, Heike Langenberg. A peer review file is available.